ELSEVIER Journal of Constructional Steel Research 57 (2001) 525–545

JOURNAL OF CONSTRUCTIONAL STEEL RESEARCH

www.elsevier.com/locate/jcsr

Ultimate strength analysis of corrugated bulkheads considering influence of shear force and adjoining structures

H.D. Ji, W.C. Cui *, S.K. Zhang

Department of Naval Architecture & Ocean Engineering, Shanghai Jiao Tong University, Shanghai 200030, People's Republic of China

Received 3 May 2000; received in revised form 2 October 2000; accepted 23 November 2000

Abstract

In this paper, simplified formulas to calculate the ultimate strength of corrugated bulkheads are derived using the beam–column theory. The formulas can take account of the influences of shear force and adjoining structures. By comparing the results from present formulas with those of other numerical analyses, it is shown that the formulas derived in this paper are accurate and reliable for engineering purposes. Thus, a more powerful design tool is provided. Finally the effects of the shear force and rigidities of adjoining structures on the ultimate strength of corrugated bulkheads are also studied.

Keywords: Ultimate strength; Corrugated bulkhead; Beam–column; Elastically fixed rigidity

1. Introduction

The bulk carrier, long recognized as the workhorse of the world merchant fleet, has over the years had its design refined and optimized on the basis of previous successful experience. However, recently, a series of tragic ship losses with loss of human lives, has focused the attention of the marine industry and the public on the performance and inherent safety of this ship type [1].

Many studies to reduce bulk carrier casualties have subsequently been undertaken

* Corresponding author. Tel.: +86-21-62932056; fax: +86-21-62933160.
E-mail address: wccui@mail.sjtu.edu.cn (W.C. Cui).

0143-974X/01/$ - see front matter
PII: S0143-974X(00)00032-8

by major classification societies and international organizations such as the International Maritime Organization (IMO) [2], and the International Association of Classification Societies (IACS).

By extensive research and investigation, people find that one major possible cause of the loss of oceangoing bulk carriers is progressive collapse of corrugated bulkheads in a flooded condition. So, in the past few years, many people have carried out research on the ultimate strength of transverse corrugated bulkheads and several proposed simplified formulas to calculate the ultimate bending moment acting on them. But in their studies, the influence of axial compression in the bulkheads induced by global vertical shearing forces of the ship is not considered and the boundary conditions at the junction of corrugation and adjacent structures are considered as either simply supported or clamped which is not the real case.

In this paper, we attempt to make new contributions to the above two problems. First, based on the results of other previous experimental and finite element analyses [3–5], we use the single corrugation model as shown in Fig. 1 to carry out research on the ultimate strength of corrugated bulkheads and a simplified formula taking account of the axial force to calculate the ultimate bending moment which the corrugated bulkhead can resist is proposed by improving that of Paik et al. [3]. Then, using the elasto–plastic theory, a formula to predict the corresponding ultimate applied lateral pressure taking account of the influences of adjoining structures and axial compression is proposed and validated. Finally, the effects of the shear force and rigidities of adjoining structures on the ultimate strength of corrugated bulkheads are also studied.

2. Ultimate bending moment

2.1. Simplified formula proposed by Paik et al. [3]

To derive a simplified formula for predicting the ultimate bending moment for a single corrugation, Paik et al. [3] used a credible axial stress distribution over the

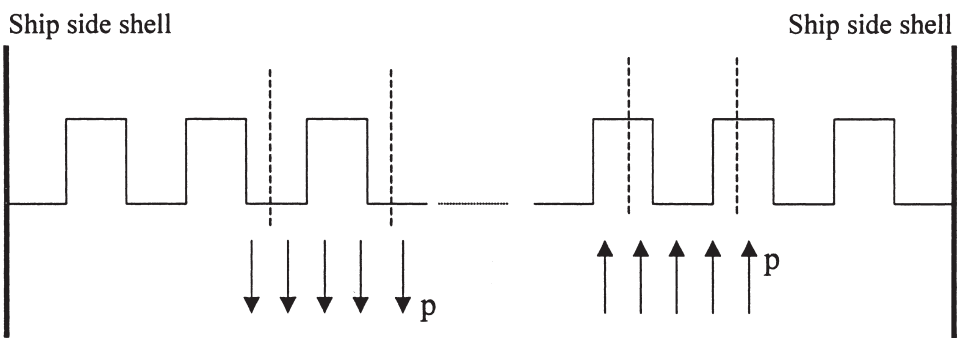

Fig. 1. Same single corrugation model used for the prediction of the ultimate strength under lateral pressure from two different sides of the transverse bulkhead.

cross section of the corrugation at the ultimate limit state, assuming that the entire material in compression of the corrugation reaches its ultimate buckling strength while the material in tension is in full yielding, see Fig. 2.

The expression for the ultimate bending moment is given as [3]:

$$M_u=\sigma_{of}\cdot A_f\cdot g+\sigma_{ow}\cdot A_w\cdot\sin\phi\cdot\frac{g^2}{d}+\sigma_{uw}\cdot A_w\cdot\sin\phi\cdot\frac{(d-g)^2}{d}+\sigma_{uf}\cdot A_f\cdot(d-g) \tag{1}$$

where A_f is the section area of corrugation flange, $a\cdot t_f$; A_w is the cross section of corrugation web, $c\cdot t_w$; d is the vertical height of corrugation web, $c\cdot\sin\phi$; and, g is the final neutral axis at ultimate limit state

$$=\frac{d[(\sigma_{uf}-\sigma_{0f})\cdot A_f+2\sigma_{uw}\cdot A_w\cdot\sin\phi]}{2(\sigma_{0w}+\sigma_{uw})\cdot A_w\cdot\sin\phi} \tag{2}$$

ϕ is the corrugation angle; σ_{0f},σ_{0w} are the tensile yield strength of corrugation flange, web, respectively; and, σ_{uf},σ_{uw} are the ultimate compressive strength of corrugation flange, web, respectively.

The ultimate compressive strength of the corrugation flange and web can be calculated by using the following empirical formula of Paik and Thayamballi [6]:

$$\frac{\sigma_u}{\sigma_0}=\frac{1}{\sqrt{0.996+0.17\beta^2}} \tag{3}$$

where σ_u is the ultimate buckling strength; σ_w for corrugation flange; σ_{uw} for corrugation web; β is the reduced plate slendernes ratio; $\beta_f=(a)/(t_f)\ \sqrt{(\sigma_{0f})/(E)}$ for corrugation flange; $\beta_w=(a)/(t_w)\ \sqrt{(\sigma_{0f})/(E)}$ for corrugation web; σ_0 is the tensile yield strength, $=\sigma_{0f}$ for corrugation flange, $=\sigma_{0w}$ for corrugation web; and t_f,t_w is the plate thickness of flange and web respectively.

2.2. Simplified method considering the influence of axial compression [5]

When there exists an axial compressive stress, the stress distribution within the section can be assumed (see Fig. 3) [7].

Since the total axial force acting on the cross section is T, this will result in the following expression:

$$\sigma_{uf}\cdot A_f-\sigma_{0f}\cdot A_f-2\sigma_{0w}\cdot t_w\cdot g'/\sin\phi+2\sigma_{uw}\cdot t_w\cdot(d-g')/\sin\phi=T \tag{4}$$

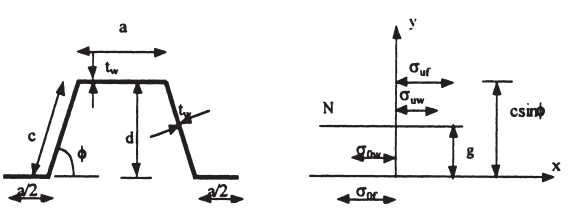

Fig. 2. Assumed distribution of longitudinal stress in corrugation cross section at ultimate collapse state (ultimate buckling in compression parts and full yielding in tension parts).

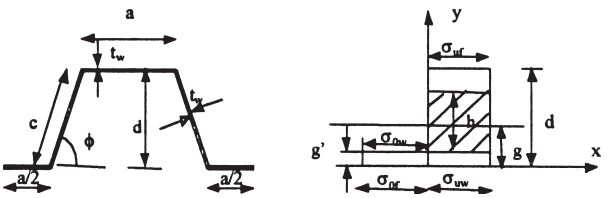

Fig. 3. Assumed distribution of longitudinal stress in corrugation cross section at ultimate collapse state considering the influence of axial compression (ultimate buckling in compression parts and full yielding in tension parts).

Then we can derive the equation to calculate the height of the area subject to tensile stress at ultimate limit state:

$$g' = \frac{d[(\sigma_{uf} - \sigma_{0f}) \cdot A_f + 2\sigma_{uw} \cdot A_w - T]}{2(\sigma_{0w} + \sigma_{uw}) \cdot A_w} \tag{5}$$

It may be worth pointing out here that there is a difference between Eq. (5) and Eq. (2) even in the case of T=0. In Eq. (2), the web area was projected to the vertical direction while in Eq. (5), the total web area is used.

Then the final neutral axis at ultimate limit state can be given by:

$$g = g' + h/2 \tag{6}$$

where h is the height of area subject to stress induced by axial compression T

$$= T \cdot \sin\phi / 2t_w\sigma_{uw} \tag{7}$$

Finally, we can derive the equation to calculate the ultimate bending moment considering the axial compression:

$$M_u = \sigma_{0f} \cdot A_f \cdot g + \sigma_{uf} \cdot A_f \cdot (d-g) + 2\int_{h/2}^{g} \sigma_{0w} \cdot t_w \cdot y / \sin\phi \, dy + 2\int_{h/2}^{d-g} \sigma_{uw} \cdot t_w \cdot y / \sin\phi \, dy \tag{8}$$

$$= \sigma_{0f} \cdot A_f \cdot g + \sigma_{uf} \cdot A_f \cdot (d-g) + \sigma_{0w} \cdot t_w \cdot \frac{g'^2 + g'h}{\sin\phi} + \sigma_{uw} \cdot t_w \cdot \frac{(d-g')^2 - (d-g') \cdot h}{\sin\phi}$$

The derivation above is under the premise that g' is larger than the thickness of corrugation web t_w. If $g' < t_w$, Eqs. (4), (5) and (7) must be replaced by Eqs. (9)–(11):

$$\sigma_{uf} \cdot A_f - \sigma_{0f} \cdot a \cdot g' + \sigma_{uf} \cdot a \cdot (t_w - g') + 2\sigma_{uw} \cdot t_w \cdot c = T \tag{9}$$

$$g' = \frac{d[(\sigma_{uf} - \sigma_{0f}) \cdot A_f + 2\sigma_{uw} \cdot A_w - T]}{2(\sigma_{0w} + \sigma_{uw}) \cdot A_w} \tag{10}$$

h=the height of area subject to stress induced by axial compression T

$$=\frac{[T-\sigma_{uf}\cdot a\cdot(t_w-g')]\cdot\sin\phi}{2t_w\cdot\sigma_{uw}} \tag{11}$$

If the result of Eq. (11) is less than d, then we can use Eqs. (13) and (14) to calculate g and M_u.

According to the theory that the stress induced by axial force will not contribute to the bending moment, we can obtain Eq. (12):

$$2h\cdot t_w\cdot\sigma_{uw}/\sin\phi\cdot(h/2-g)-\sigma_{uf}\cdot a\cdot(t_w-g')\cdot g=0 \tag{12}$$

Then the equation to calculate g and M_u is obtained:

$$g=\frac{h^2\cdot t_w\cdot\sigma_{uw}}{2h\cdot t_w\cdot\sigma_{uw}+\sigma_{uf}\cdot a\cdot(t_w-g')\cdot\sin\phi} \tag{13}$$

$$M_u=\sigma_{0f}\cdot a\cdot g\cdot g'+\sigma_{uf}\cdot A_f\cdot(d-g)+2\int_{h-g}^{d-g}\sigma_{uw}\cdot t_w\cdot y/\sin\phi dy=\sigma_{0f}\cdot a\cdot g\cdot g'+\sigma_{uf}\cdot A_f\cdot(d \tag{14}$$

$$-g)+\sigma_{uw}\cdot t_w\cdot\frac{(d-g)^2-(h-g)^2}{\sin\phi}$$

If h, calculated by Eq. (11), is larger than d, we can see that the area of stress subject to axial force has expended to the upper flange. Then g and M_u can be obtained by:

$$2c\cdot t_w\cdot\sigma_{uw}\cdot(d/2-g)+a\cdot x\cdot\sigma_{uf}\cdot(d-g)-\sigma_{uf}\cdot a\cdot(t_w-g')\cdot g=0 \tag{15}$$

$$g=\frac{c\cdot t_w\cdot\sigma_{uw}\cdot d+a\cdot x\cdot\sigma_{uf}\cdot d}{2c\cdot t_w\cdot\sigma_{uw}+a\cdot x\cdot\sigma_{uf}+\sigma_{uf}\cdot a\cdot(t_w-g')} \tag{16}$$

where x=height of area in upper flange subject to stress induced by axial force

$$=\frac{T-2c\cdot t_w\cdot\sigma_{uw}=\sigma_{uf}\cdot a\cdot(t_w-g')}{\sigma_{uf}\cdot a} \tag{17}$$

$$M_u=\sigma_{uf}\cdot(t_w-x)\cdot(d-g)+\sigma_{uf}\cdot g\cdot g'$$

2.3. Flow chart

The procedure for calculating the ultimate bending moment acting on the single corrugation can be represented by the flow chart shown in Fig. 4.

2.4. Influence of axial compression on the ultimate bending moment

To investigate the influence of axial force on the ultimate bending moment, we define

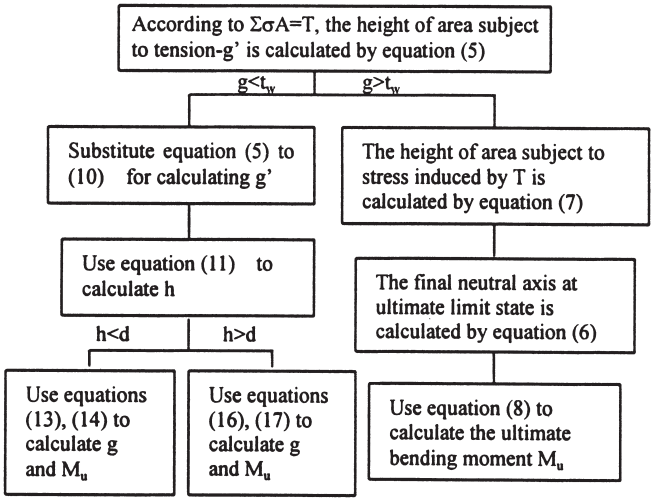

Fig. 4. Flow chart to calculate ultimate bending moment.

$$k=\sqrt{\frac{T}{EI}}$$

to replace T, then the influence is shown in Fig. 5. When kL=0, the ultimate bending moment will be the same as that of Paik's result for ϕ=90°. However, if ϕ<90°, there will be some difference. For example, if the corrugation angle of model P90-1 whose dimensions are shown in Table 1 is changed into 60°, then $M_{u\ present}/M_{u\ Paik}$=1.06.

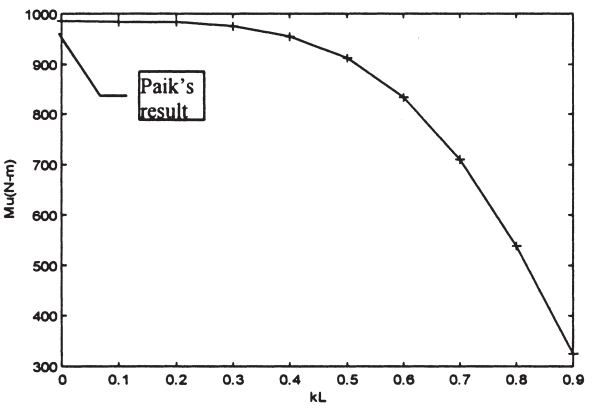

Fig. 5. Ultimate bending moment varying axial force.

Table 1
Dimensions of corrugated bulkhead models

Specimen no.	1 (mm)	B (mm)	a (mm)	t_f (mm)	c (mm)	t_w (mm)	ϕ (deg.)	σ_0 (kg/mm^2)	σ_T (kg/mm^2)	E (kg/mm^2)	I ($\times 10^6$mm^4)	β_f	β_w
90-1	1219	750	74.7	0.81	74.6	0.81	89.1	19.03	29.21	1.880	0.217	2.934	2.930
90-2	1219	750	75.3	1.19	74.8	1.19	88.0	18.15	30.16	1.870	0.323	1.971	1.958
90-3	1219	750	75.1	1.59	74.9	1.59	87.5	27.47	35.09	2.090	0.418	1.712	1.708
60-1	1219	1125	74.5	0.81	75.1	0.81	58.1	19.03	29.21	1.880	0.158	2.926	2.950
60-2	1219	1125	74.9	1.19	74.5	1.19	58.1	18.15	30.16	1.870	0.224	1.961	1.950
60-3	1219	1125	74.8	1.59	74.2	1.59	57.9	27.47	35.09	2.090	0.290	1.706	1.692

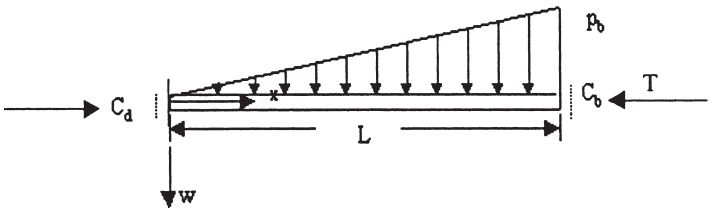

Fig. 6. Single corrugation under the combined load of lateral pressure and axial compression.

3. Ultimate pressure load prediction

From the above formulations, we can calculate the ultimate bending moment at the ultimate limit state for the corrugated cross section. To predict the corresponding ultimate applied pressure load it is necessary to establish the relationship between the applied pressure loads and the bending moments at the ultimate limit state. In the following, we derive such a relationship using the beam–column theory.

Fig. 6 represents a single corrugation model that is a proxy for the behavior of a corrugated bulkhead subject to lateral hydrostatic pressure and axial compression. Fig. 7 shows the elastic bending moment distribution under these loading and fixed conditions.

The lateral hydrostatic pressure distribution with a triangular pattern is assumed to vary linearly between the bottom and deck structures, with the magnitude of pressure per unit length related to single corrugation as follows:

$$p = p_b \frac{x}{L}$$

where p_b is the lateral pressure at the lower (bottom) end of the corrugation.

In some references such as Paik et al. [3,4], a more general trapezoidal pattern of pressure load is used. This will bring little difficulty for the derivation of the solution. But in most of the practical applications [2,5], the triangular pattern has often been employed for the distribution of the bulkhead's pressure load and therefore this pattern is chosen for study in this paper.

The lateral deflection can be given by solving the following differential equation using the initial parameter method [8]:

$$EIw^{IV} + Tw'' = p \tag{18}$$

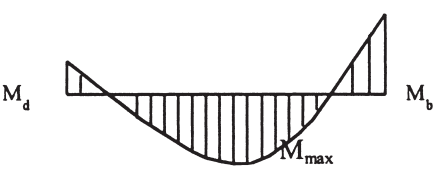

Fig. 7. Elastic bending moment distribution.

$$w=w_0+\frac{\theta_0}{k}\sin kx+\frac{M_0}{EIk^2}(1-\cos kx)+\frac{N_0}{EIk^3}(kx-\sin kx)+\int_0^x\frac{p(\xi)d\xi}{EIk^3}[k(x-\xi) \quad (19)$$

$$-\sin k(x-\xi)]$$

where

$$p(\xi)=p_b\frac{\xi}{L}$$

I=moment of inertia of the beam; E=Young's modulus.

The four parameters in Eq. (19) can be obtained by considering the following end conditions:

$$w(0)=0$$
$$w(L)=0 \quad (20)$$

$$EI\left(\frac{d^2w}{dx^2}\right)_{x=0}=C_d\left(\frac{dw}{dx}\right)_{x=0}$$
$$EI\left(\frac{d^2w}{dx^2}\right)_{x=L}=-C_b\left(\frac{dw}{dx}\right)_{x=L} \quad (21)$$

where C_b and C_d are elastically fixed rigidities at the lower and upper ends of the corrugation, respectively.

Then the equation to calculate bending moment is expressed as follows:

$$M=EI\frac{d^2w}{dx^2}=[(-EIk\sin kx+C_d\cos kx)\theta_0+\frac{\sin kx}{k}N_0+\frac{1}{k^3L}(kx-\sin kx)]\cdot p_b \quad (22)$$

The extreme value of the bending moment inside the span will occure at the location where the following condition is satisfied:

$$\frac{dM}{dx}=0 \quad (23)$$

Then the maximum bending moment in the middle region and the bending moment at the lower end can be given by:

$$M_{max}=EI\frac{d^2w}{dx^2}=(-EIk\sin kx_p+C_d\cos kx_p)\theta_0+\frac{\sin kx_p}{k}N_0+\frac{1}{k^3L}(kx_p-\sin kx_p) \quad (24)$$

where x_p=the location at which the maximum bending moment occurs.

$$M_b=EI\frac{d^2w}{dx^2}=(-EIk\sin kL+C_d\cos kL)\theta_0+\frac{\sin kL}{k}N_0+\frac{1}{k^3L}(kL-\sin kL) \quad (25)$$

To facilitate the research below, C_b and C_d are non-dimensionalized:

$$C_B=C_b\cdot\frac{L}{EI},\ C_D=C_d\cdot\frac{L}{EI}$$

Compare M_{max} and M_b, here a critical elastically fixed rigidity C_{BC} is introduced at which $M_{max}=M_b$. When C_D is constant, M_{max} will be less than M_b if C_B is larger than C_{BC}, vice versa.

3.1. $C_B>C_{BC}$

In this case, M_{max} is less than M_b and it represents that the bending moment at the bottom end will first reaches the ultimate bending moment of the beam cross section and the plastic hinge will first formed at the bottom end, see Fig. 8.

So, the end condition will change into:

$$\begin{aligned} &w(0)=0\\ &w(L)=0\\ &EI\left(\frac{d^2w}{dx^2}\right)_{x=0}=C_d\left(\frac{dw}{dx}\right)_{x=0}\\ &EI\left(\frac{d^2w}{dx^2}\right)_{x=L}=M_u \end{aligned} \tag{26}$$

Also, the in-span maximum bending moment M_{max} will be developed at the location where:

$$\frac{dM}{dx}=0$$

and the maximum bending moment can be obtained by:

$$M_{max}=EI\frac{d^2w}{dx^2}=(-EIk\sin kx_p+C_d\cos kx_p)\theta_0+\frac{\sin kx_p}{k}N_0+\frac{p_b}{k^3L}(kx_p-\sin kx_p) \tag{27}$$

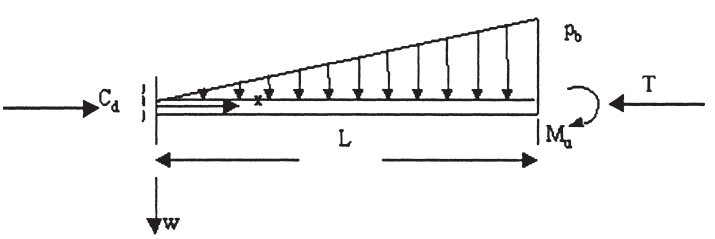

Fig. 8. Single corrugation under the combined load of lateral pressure and axial compression when a plastic hinge is formed at the bottom end.

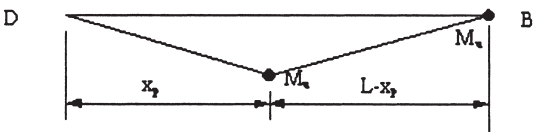

Fig. 9. Assumed collapse hinge mechanism.

Increase p_b until M_{max} reaches M_u, then there will be two plastic hinges formed at the middle and the bottom end of the beam respectively, see Fig. 9. Theoretically, in this case, a collapse hinge mechanism is not formed, the beam still has some carrying capability. But according to the result of the finite element analysis by Konish [5], the corrugated bulkhead can be considered to collapse after two plastic hinges are formed. So, in this paper, we will not do any further analysis and consider this case to be the ultimate limit state. The present p_b is considered the ultimate lateral pressure.

3.2. $C_B < C_{BC}$

In this case, M_{max} is larger than M_b and it represents the bending moment at the middle of the beam which first reaches the ultimate bending moment of the beam cross section and the plastic hinge will first be formed at the bottom end, see Fig. 10.

To obtain the expression of the bending moment at the bottom end, the beam is separated into two parts, the end conditions of the left part are:

$$w(0)=0$$

$$EI\left(\frac{d^2w}{dx^2}\right)_{x=0}=C_d\left(\frac{dw}{dx}\right)_{x=0}$$

$$EI\left(\frac{d^2w}{dx^2}\right)_{x=x_p}=-M_u$$

and the end conditions of the right end are:

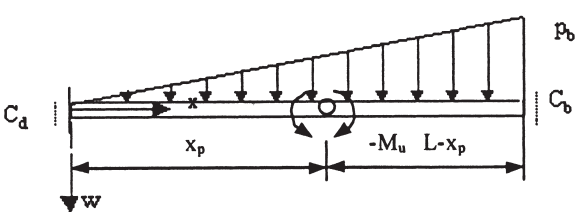

Fig. 10. Single corrugation under the combined load of lateral pressure and axial compression when a plastic hinge is formed at the middle of the beam.

$$w(L)=0$$

$$EI\left(\frac{d^2w}{dx^2}\right)_{x=x_p}=-M_u$$

$$EI\left(\frac{d^2w}{dx^2}\right)_{x=L}=-C_b\cdot\left(\frac{dw}{dx}\right)_{x=L}$$

The following continuity conditions at the plastic hinge location of $x=x_p$ should also be considered:

$$(N_{x=xp})_{left}=-(N_{x=xp})_{right}$$

$$(w_{x=xp})_{left}=(w_{x=xp})_{right}$$

where $(N_{x=xp})_{left}$, $-(N_{x=xp})_{right}$ are the shearing forces calculated by the formulas of the left part and right part of the beam.

Then, the bending moment at the bottom end, M_b can be obtained by:

$$M_b=EI\frac{d^2w}{dx^2}(x=L)$$

First, we also assume that a plastic hinge is formed at the bottom end when M_b reaches ultimate bending moment M_u and the lateral pressure then will be the ultimate lateral pressure. Fig. 11 shows the effect of C_B on the ultimate lateral pressure thus defined and from this figure, it can be seen that as long as the elastically fixed rigidity

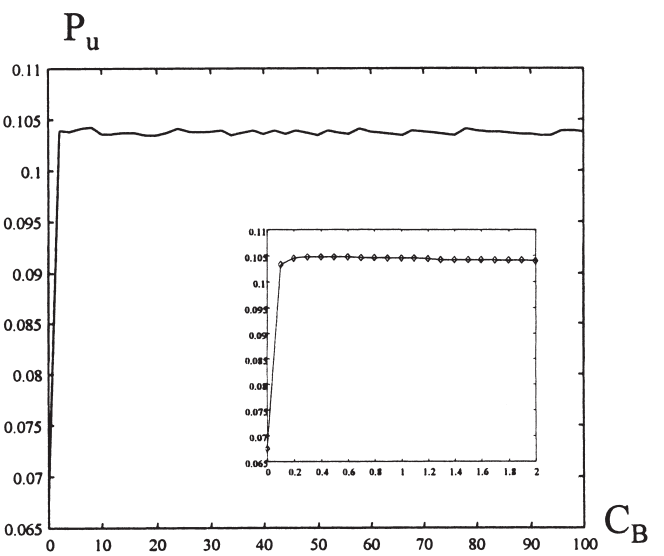

Fig. 11. Ultimate lateral pressure varying with critical constrain constant at the bottom end.

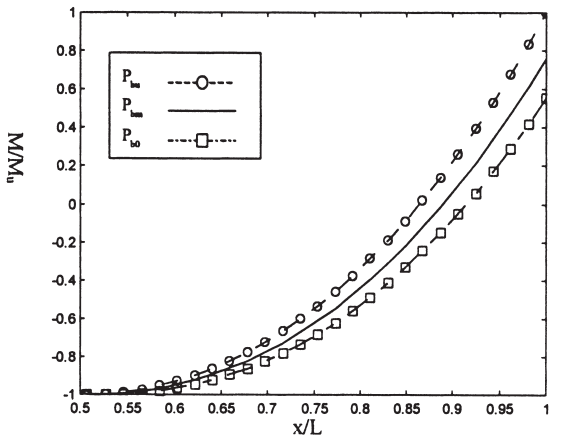

Fig. 12. Distribution of bending moment along the length of the beam under different lateral pressure when C_B is less than C_{BC}.

C_B is larger than zero, even it is very small, the ultimate lateral pressure will be the same as the one under the condition that $C_B=\infty$, this is apparently unreasonable.

Next, let us compare the bending moment distribution under $C_B<C_{BC}$ (Fig. 12) with that under $C_B>C_{BC}$ (Fig. 13). In these two figures, p_{b0} is the lateral pressure under which the first plastic hinge is formed, p_{bu} is the lateral pressure under which two plastic hinges are formed, p_{bm} is the lateral pressure between p_{b0} and p_{bu}.

From Fig. 12, we can see that when the first plastic hinge is formed at the middle of the corrugation beam, quite a large part of the beam will be subjected to high bending moment. As the applied lateral pressure increases, the increase of the bending moment at the bottom end is not very quick. Therefore, for a pressure level

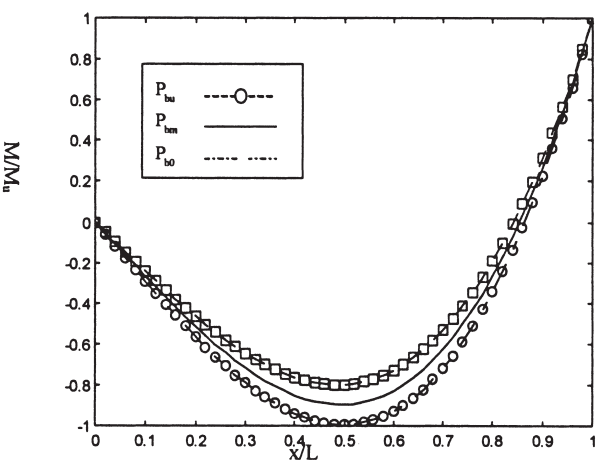

Fig. 13. Distribution of bending moment along the length of the beam under different lateral pressure when C_B is larger than C_{BC}.

$p_{b0}<p_b<p_{bu}$, the yielding zone in the middle location is actually quite large. However, due to the strict end conditions, this cannot be reflected. Therefore, the validity of the solution for the bending moment distribution under $C_B<C_{BC}$ and $p_b>p_{b0}$ is questioned. In Fig. 13, the bending moment at the bottom end (yielding zone) will not spread and therefore, this bending moment is reasonable. Because of this reason, it is assumed in this paper that when $C_B<C_{BC}$, the ultimate limit state is reached when one plastic hinge is formed at the middle of the corrugation.

4. Validation of the formula

4.1. Compared with the theoretical results of Paik et al. [3,4]

First, the formulas in this paper can be considered as an extension of those of Paik et al. [3,4]. When T=0, they should be degenerated into those of Paik et al. Fig. 14 shows the effect of axial force on the ultimate lateral pressure under the end condition of $C_B=\infty$, $C_D=0$. The dimensions of model 90-1 and other models are given in Table 1.

According to the formulas derived by Paik et al. [4], in the case of T=0, the ultimate lateral pressure at the bottom end can be estimated by:

$$P_{bu}=\frac{12L-6x_p}{2L^2x_p-3Lx_p+x_p^3}\cdot M_u=0.104 \text{ MPa} \tag{28}$$

From Fig. 14, we can see that the results calculated by the formulas of this paper

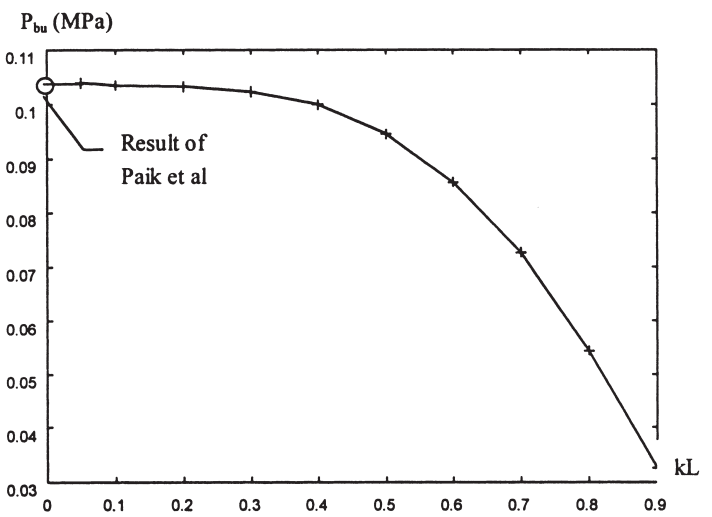

Fig. 14. Effect of axial compression on the ultimate lateral pressure.

can be successfully degenerated into that of Paik et al. and therefore these formulas are validated in one aspect.

4.2. Comparison with FEA results of Konish et al. [5]

Next, we will compare our results with the FEA results of Konish et al.,[5] Konish et al. have used half-pitch corrugation model under simply supported end conditions. The lateral force is uniformly distributed. From Table 2, we can see that the results of our formulas are very close to those of Konish et al., and the formulas of this paper are simpler in the sense that no correction is needed for the influence of gusset plates and shedder plates.

4.3. Comparison with our own FEA results [6]

Since there are little previous results which have taken into account the influence of axial compression, to make further validation of the formulas of this paper, we use half pitch model 90-1 whose dimensions are shown in Table 1 to build FEM models. The end condition is one end simply supported and the other end clamped. Lateral pressure is uniformly distributed and an axial compressive force exists. The FEA is carried out using MSC/NASTRAN and the displacement of the FE mesh model at the ultimate state is shown in Fig. 15.

The results are shown in Table 3. It can be found that as kL increases the difference between FEA and the proposed formulas increases. This indicates that the present model is more applicable for the small axial load cases. In a preliminary study for a ship of 71 000 DWT bulk carrier [6], the maximum axial compression kL induced by the maximum global shearing forces is 0.315. Therefore, for practical application the proposed formulas are credible and can be used as a tool to calculate the ultimate strength of corrugated bulkheads on the bulk carriers.

5. Influence of axial compression and fixed rigidity on the ultimate strength of corrugated bulkheads

5.1. Influence of axial compression

From Fig. 14, we can see that the apparent influence of axial compression on the ultimate strength, especially when kL is larger than 0.4, the value of ultimate lateral pressure decreases rapidly with the increase of kL. By the analysis of the axial compression induced by shearing force of the corrugated bulkhead of one 71 000 dwt bulk carrier [6], we found that the value of kL is about 0.3, at this value the ultimate lateral pressure is about 97% of the one under no influence of axial compression. So, whether we should take into account the influence of axial compression is dependant on the specific condition. To make a decision, we may carry out some analysis using the method of this paper.

Besides these, the value of axial compression also has a certain influence on the

Table 2
Comparison of collapse water heads of present formulas with the proposed formula of Konish et al. and their FEM results

Ship No.	A	B	C	D	E	F	G	H	I	J	K	L	M	N	O	P	Q	R	R′
Konish Formula	10.3	18.7	10.3	9.3	16.6	9.6	13.5	9.0	16.2	10.0	13.5	11.3	15.2	12.2	8.1	8.1	10.1	12.7	12.1
Konish FEM	10.8	17.4	12.3	10.3	19.2	9.9	15.1	9.3	18.8	10.9	15.0	12.9	16.4	13.9	12.2	9.4	11.5	12.9	14.0
Present formula	9.2	21.6	10.9	11.9	17.6	8.7	14.3	10.8	16.5	11.8	13.5	12.1	16.6	9.2	11.4	7.6	9.0	12.4	12.4

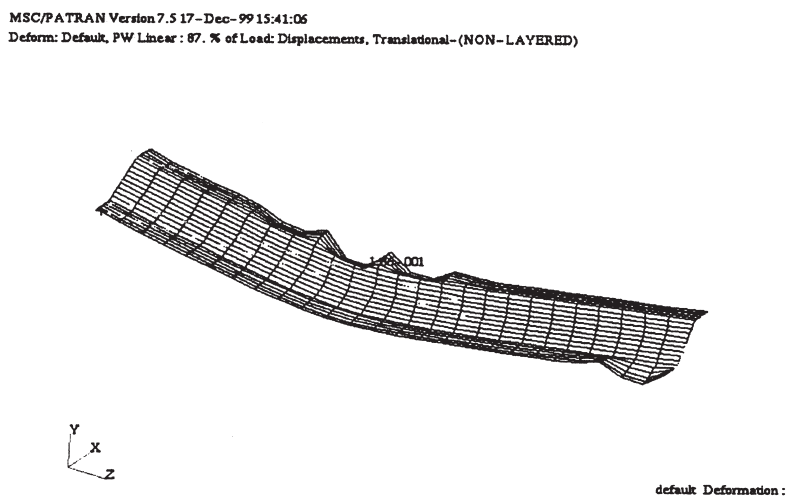

Fig. 15. Displacement of half-pitch model at ultimate limit state.

Table 3
Comparison with FEA

kL	Ultimate lateral pressure (kg/cm^2)	
	FEA	Proposed formula
0.49	0.46	0.462
0.574	0.42	0.431
0.63	0.38	0.399
0.699	0.33	0.353

location of the plastic hinge and the critical elastically fixed rigidity. These will be discussed later in this paper.

5.2. Influence of elastically fixed rigidity of bottom end

5.2.1. Critical elastically fixed rigidity

From the derivation process above, we can see that the definition of critical elastically fixed rigidity is very important. When the value of critical elastically fixed rigidity is known, we can presume the mode of plastic mechanism of the corrugation beam, and thereby predict the ultimate lateral pressure. Fig. 16 shows the curve of critical elastically fixed rigidity versus the axial compression, and by curve fitting technique, the general relationship between critical elastically fixed rigidity and the axial compression is obtained:

$$C_{BC}=4.9972-0.01116(kL)+0.14195(kL)^2 \tag{29}$$

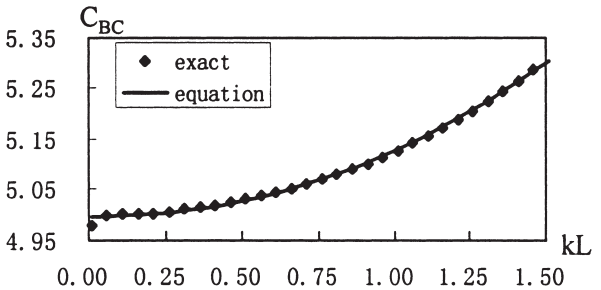

Fig. 16. Effect of kL on the critical elastically fixed rigidity C_{BC}.

The equation above fits well with the theoretical results and from this equation we can see that the value of C_{BC} is approximately 5.

5.2.2. The location of plastic hinge

To carry out further analyses of the influence of axial compression and the elastically fixed rigidity on the location of the in-span plastic hinge, we use the dimensions of model 90-1, varying the value of kL and C_B to calculate the location of in-span plastic hinge under the end condition: C_D=0. Fig. 17 shows that the location of plastic hinge moves farther from the bottom end when C_B increases. It can also be seen that this will also happen when the value of axial compression increases, but the effect is so small that it can be ignored.

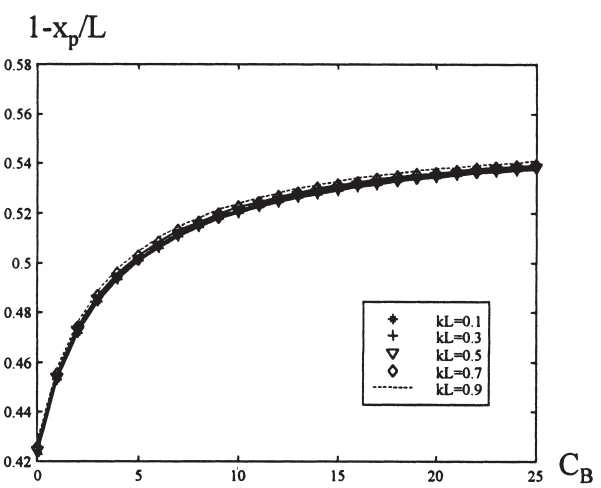

Fig. 17. The location of plastic hinge varying with the value of elastically fixed rigidity of the bottom end under different axial compressions.

5.2.3. Influence on the ultimate lateral pressure

From Fig. 17, we can see that the minimum value of lateral pressure is developed when C_D=C_B=0, i.e. both ends are simply supported. Then it will increase with C_B until C_B reaches the critical value. Thereafter, it will remain almost constant.

5.3. Influence of the elastically fixed rigidity of the upper end

The above discussions are all under the assumption that the beam is simply supported at the upper end. In the following, the influence of the elastically fixed rigidity of the upper end is studied. Fig. 18 shows the curve of ultimate lateral pressure versus C_D when kL=0.5, C_B=10^6.

Since the value of C_D is much less than C_B, in Fig. 19, we confine it between 0 and 4. From Fig. 19, we can see that the value of p_{bu} also increases with C_D which can be easily explained, but the extent of change is not as big as that of Fig. 18. The influence of the elastically fixed rigidity at the upper end may also be taken into account for accurate analysis.

6. Concluding remarks

Due to the occurrence of several bulk carrier losses during the last decade, the safety assessment of bulk carrier corrugated bulkheads has been of interest, and most recently, bulk carrier corrugated bulkhead requirements have been enhanced by IMO and IACS.

The enhanced requirements are aimed at predicting the ultimate strength of corrugated bulkheads subject to accidental flooding in a relatively simple and reasonably accurate manner. In fact, the adjoining structures like the deck, the upper and bottom

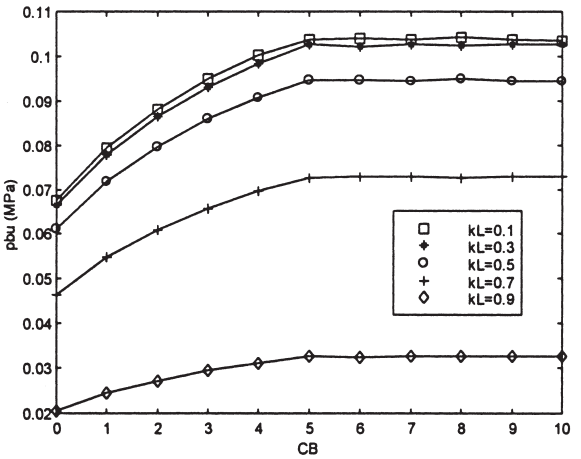

Fig. 18. Ultimate lateral pressure varying with the value of elastically fixed rigidity of the bottom end under different axial compressions.

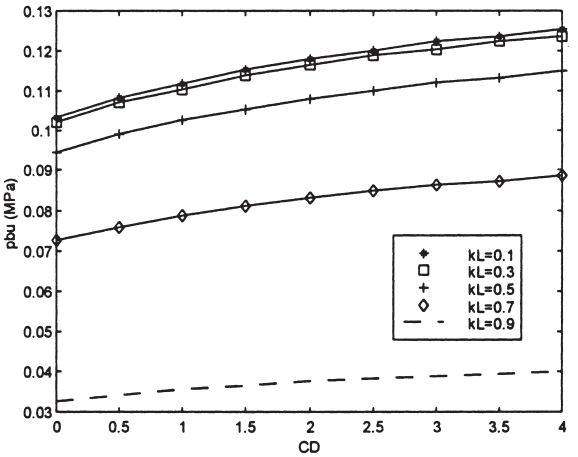

Fig. 19. Ultimate lateral pressure varying with the value of elastically fixed rigidity of the upper end under different axial compressions.

stool and also the double bottom may affect the ultimate strength of the corrugated bulkhead, which makes the actual behavior in particular cases could differ from the predictions obtained from design formulae based on idealized end condition [4]. Besides, the axial compression induced by vertical shear forces may also reduce the ultimate strength of the corrugated bulkheads. Although these two factors have been mentioned in some literatures [3], they are not thoroughly investigated.

In this paper, a simplified formula to calculate the ultimate moment of the single corrugation beam is first derived using the simple approach of Paik et al. [3], then the formulas to predict corresponding ultimate lateral pressure are also derived using the elasto–plastic theory. These formulas are validated by comparing their results with those of Paik's formulas and Konish's FEA. Finally, the influence of axial compression and end elastically fixed rigidity on the ultimate strength is studied.

From the researches carried out in this paper, the following conclusions can be drawn:

- The axial compression induced by shearing force has some effect on the ultimate strength of corrugated bulkheads which depends on ship style and load case. This paper has provided the means to estimate this effect.
- The critical value of end elastically fixed rigidity is approximately 5, its accurate value can be obtained by using Eq. (29) in this paper.
- When the elastically fixed rigidity at the bottom end is less than the critical value, only one plastic hinge can be formed in the corrugation beam when it reaches the ultimate limit state; when the elastically fixed rigidity at the bottom end is larger than the critical value, two plastic hinges will be formed at the middle and bottom end of the corrugation beam respectively when it reaches the ultimate limit state.
- When the elastically fixed rigidity at the bottom is larger than the critical value,

the ultimate lateral pressure becomes almost constant and can be estimated by using one end simply supported and clamped end condition.

- The elastically fixed rigidity at the upper end of the corrugation beam also has some influence on the ultimate strength of the corrugation bulkheads which is relatively small compared with that of the bottom end.

References

[1] Lloyd's Register. Buk carriers—an update, March 1998.
[2] RINA. New bulk carrier rules confirmed by IMO, The Naval Architect. February 1998, p. 33.
[3] Paik JK, Thayamballi AK, Chun MS. Theoretical and experimental study on the ultimate strength of corrugated bulkheads. J Ship Research 1997;41(4):301–17.
[4] Paik JK, Thayamballi AK, Kim SG. The influence of adjoining structures on the ultimate strength of corrugated bulkheads. Proc. of the 7th International Symposium on Practical Design of Ships and Mobile Units (PRADS'98), The Hague, September 1998. p. 111–24.
[5] Konishi H, Yao T, Shigemi T, Kitamura O, Fujikubo M. Design of corrugated bulkhead of bulk carrier against accidental flooding load. Proc. of the 7th International Symposium on Practical Design of Ships and Mobile Units (PRADS'98), The Hague, 1998. p. 157–63.
[6] Paik JK, Thayamballi AK. An empirical formulation for predicting the ultimate compressive strength of stiffened panels. Proc. of the 7th International Offshore and Polar Engineering Conference, Vol. 4, Honolulu, May 1997. p. 328–38.
[7] Ji HD. Research on the ultimate ultimate strength of corrugation bulkheads on bulk carriers. Master's thesis, Department of Naval Architecture and Ocean Engineering, Shanghai Jiao Tong University, 2000 (in Chinese).
[8] Chen BZ, Chen TY. Ship structural mechanics. Shanghai Jiaotong University Publishing Company, 1990 (in Chinese).